Substrate-Induced Phase Transitions in Thin Films of Cylinder-Forming Diblock Copolymer Melts

Larisa Tsarkova,* Armin Knoll,† Georg Krausch, and Robert Magerle‡

Physikalische Chemie II, Universität Bayreuth, D-95440 Bayreuth, Germany

Received January 30, 2006; Revised Manuscript Received March 6, 2006

ABSTRACT: Terrace formation and morphological behavior in thin films of polystyrene-*block*-polybutadiene block copolymer have been studied on two chemically different substrates by means of scanning force microscopy. Cylinders parallel to the film plane ($C_{||}$) are found on weakly interacting substrates in up to five-layer-thick films. A bottom layer of half cylinders is stabilized at the substrate. On strongly interacting substrates, the development of the $C_{||}$ microdomains and nonbulk perforated lamella (PL) and lamella (L) phases depends on the local film thickness. The sequence of structures at transition thickness (in between the steps) suggests a few percent increase of the characteristic microdomain spacing in the order $C_{||}$−PL−L. Comparison of the interlayer distances on the two types of substrates points to lamella-like structures in bulk of the films on strongly interacting surfaces.

Introduction

Ordered microstructures of block copolymers in thin films have been intensively studied over the past decades.[1−5] The interest in nanopatterned surfaces is due to their potential for technological applications such as templates for inorganic composites[6,7] or lithographic processes.[8−11] To design and process such materials, it is essential to understand their behavior in thin films.

In most of the reported research on thin block copolymer films, lamella-forming systems have been considered.[4] However, these findings are only partially confirmed for compositionally asymmetric block copolymers. The thickness-dependent structuring of the free surface, known as terrace formation, was first observed on lamella-forming films,[4,12−15] and has been only lately reported for cylindrical[16−25] and spherical[26,27] domains. Whenever the film thickness is not commensurable with the characteristic domain spacing, macroscopic regions with distinct film thicknesses ("terraces") develop upon thermal annealing or solvent annealing.

The effect of wetting conditions[4] and the energetic/chemical nature of the surfaces[28,29] on lamellae ordering in thin films is relatively well understood. A strongly interacting interface is enriched by a selectively adsorbing block; the near-surface morphology is affected as a result. A weakly interacting interface attracts none of the blocks to a significant extent and has been shown to favor the vertical orientation of lamella.[30−33] A noninteracting interface such as air, an inert gas, or vacuum, in addition to surface tension,[13,34] introduces undulational instability[35] and accelerates segmental motion.[36]

For cylinder-forming block copolymers, surface field effects have been considered theoretically.[37−42] Simulations using dynamic density functional theory (DDFT) suggest that the surfaces may initiate transitions from a hexagonal to a lamella phase in the case of sufficiently strong surface interactions.[38,41] For weak surface interactions, the parallel or perpendicular alignment of the cylinders is predicted to be dependent on the commensurability of the film thickness to the bulk spacing of the cylindrical domains.[42] The parallel-oriented cylinders either terminate with half cylinders or with a wetting layer of the block, which is preferentially attracted to the surface.[38,43] Recent calculations indicate that a significant change in the film morphology occurs even for a small change in external parameters if the block copolymer composition is close to the borderline between two different bulk phases.[39] In the self-consistent mean field approach, the surfaces are allowed to modify the Flory−Huggins interaction parameter and the chemical potential in the adjacent copolymer layer.[44]

Most of the above predictions on the surface field-regulated phase behavior in cylinder-forming block copolymers have not been supported by experiments due to the limited number of studies utilizing chemically different substrates. Harrison et al.[45] have used a layer of a random block copolymer and a polymer brush to tune the wetting conditions of a single layer of cylindrical microdomains. The variation of the interfacial interactions at the polymer/substrate interface in solvent-swollen films of a triblock copolymer[46] and terpolymer[47] seems to be insufficient, as the solvent significantly screens the presence of the substrate. The development of the nonbulk perforated lamella (PL) in up to six-layer-thick films has been attributed to the strong attraction of the minority component to the substrate.[25] However, layering of the compositionally asymmetric block copolymers under different wetting conditions has not been studied systematically so far.

The published theoretical and experimental work on thickness-dependent structures in thin films of asymmetric block copolymers indicates a much richer phase behavior than that produced by bulk melts. Despite the extensive research on the phase behavior of block copolymers in thin films, there are only a few conclusive observations that can be applied to block copolymer films in general. Most of the reported observations are restricted to the systems under investigation. It is difficult to make general conclusions about the effect of the surface fields as there is no well-determined quantitative measure of this parameter in experiments. Often it is the molecular weight, composition, molecular architecture, and annealing/quenching conditions that determine the unique thin film behavior of a given block copolymer.

* To whom correspondence should be addressed. E-mail: larisa.tsarkova@uni-bayreuth.de.

† Present address: IBM Research GmbH, Säumerstrasse 4, CH-8803 Rüschlikon, Switzerland.

‡ Present address: Technische Universität Chemnitz, Chemische Physik, D-09107 Chemnitz, Germany.

10.1021/ma060224n CCC: $33.50
Published on Web 03/30/2006

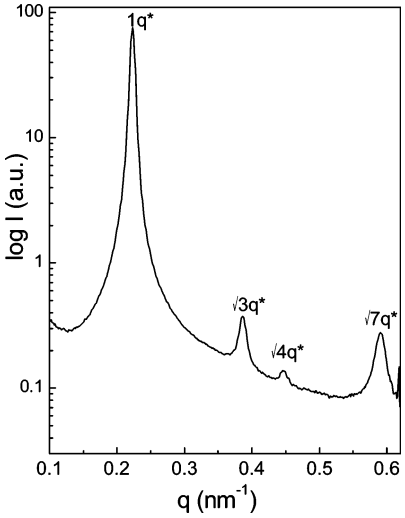

Figure 1. SAXS profile of an SB melt annealed at 120 °C for 18 h.

In this work, we study the surface topography, the phase behavior, and the energetically favored terrace heights in thin films of a cylinder-forming polystyrene-*block*-polybutadiene (SB) diblock copolymer melt as a function of the film thickness and the surface field at the substrate. The paper is organized as follows: First we present the results on the macro- and microstructure development in the topmost layer of SB films supported by two chemically different substrates. Next, we quantitatively evaluate the interlayer period for each of the substrates. Then, we relate the regions of the observed morphologies to the distinct film thickness and to particular wetting conditions. In the Discussion Section, we compare the experimentally observed and the predicted phase behavior. Finally, we suggest a model of the thickness-dependent morphological behavior on strongly interacting substrates.

Experimental Section

Polymer. The material under study is a polystyrene (PS)-*block*-polybutadiene (PB) diblock copolymer (SB), with the molecular weights of the blocks $M_{w,PS}$ =13.6 kg/mol and $M_{w,PB}$ = 33.7 kg/mol (Polymer Source Inc.) and a volume fraction of PS f_{PS} = 25.5%. The glass transition temperatures of the SB components are $T_{g,PB}$ = −60 °C and $T_{g,PS}$ = 80−100 °C.[48] The surface tension of PB, γ_{PB} = 31 mN/m, is considerably smaller than the surface tension of PS, γ_{PS} = 41 mN/m,[48] which drives PB to segregate to the free surface.

Small-Angle X-ray Scattering (SAXS). For the characterization of the bulk morphology, SAXS measurements were carried out at room temperature by using the ID02 beamline at the European Synchrotron Radiation Facility (Grenoble, France). The operating beam energy was 12.5 keV. The 1-mm-thick SB sample was annealed at 120 °C for 18 h under vacuum and cooled to room temperature. In bulk, SB forms PS cylinders in a PB matrix. Throughout the paper, the term "nonbulk" describes noncylindrical morphologies, which are not observed as an equilibrium phase in the bulk of SB melts. The characteristic spacing a_o = 32.6 ± 0.3 nm of PS cylinders was calculated from the first-order reflection in Figure 1 at q^* = 0.22 nm ($a_o = 2\pi/q^*$).

Substrates. Two types of substrates have been used in the present study. *Silicon substrates* were cut from the same base sheet of a silicon wafer (⟨100⟩ orientation, Wacker Siltronic AG), treated with fresh 3:1 H_2SO_4 (concentrated)/H_2O_2 (30%) piranha solution to form a clean silicon oxide surface, then extensively rinsed with hot water, followed by cold Millipore water and then dried. The thickness of the silicon oxide (SiO_x) surface layer prepared according to the above procedure was 1.5−2 nm (as measured with ellipsometry). We note that systematic cleaning of the silicon wafers is crucial for the reproducibility of the results.

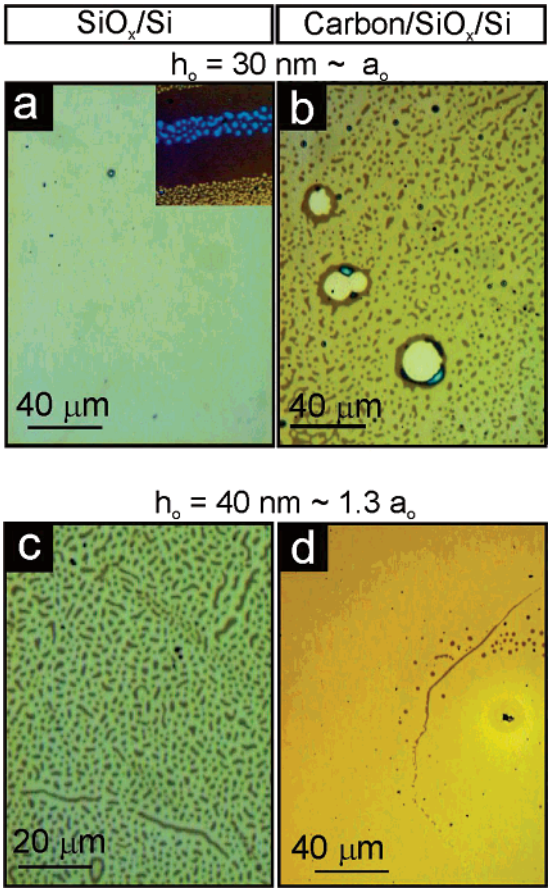

Figure 2. Optical images showing representative regions of the surface topography in SB films annealed on silicon oxide (a, c) and carbon-coated (b, d) substrates. The initial film thickness h_o and the corresponding ratio to the characteristic domains spacing a_o are indicated above each image. Differences in the terrace thickness are visible due to white light interference. Inset in (a) displays the area at the rim of the film, where it splits into terraces.

A 6 ± 1 nm *carbon* layer was evaporated onto a silicon wafer by using a Cressington 208HR sputter coater. Earlier studies suggest that the silicon oxide is preferentially wet by the PB,[49] while the low-surface-energy carbon coating is supposed to be less preferential for SB blocks than the silicon oxide and, presumably, establishes a nearly neutral substrate for both blocks.

Sample Preparation. Thin SB films were spun cast onto silicon- or carbon-coated substrates from toluene solution with the stabilizer (2,6-di-*tert*-butyl-*p*-cresol) added in the amount of 0.03% of the polymer weight to prevent cross linking of PB during thermal annealing. The initial film thickness was controlled by the concentration of the spread solution. Spin-coating of solutions with 0.25, 0.5, 0.75, 1, 1.24, 1.5, 1.7, 2.0, and 2.4 wt % of SB at a spinning rate of 2000 rpm produced films with thicknesses of 9, 20, 30, 40, 55, 68, 80, 105, and 125 nm, respectively, with ±2 nm reproducibility. We note that a thickness variation of ∼5−10% is created in each sample by the spin-coating procedure. The thickness increases from the center toward the edges of the substrate, where up to three consecutive layers of structures are formed within an area of some tens of μm^2 (inset of Figure 2a). Solvent-free SB films were annealed on different substrates simultaneously in a vacuum for 18 h at 393 K. At this temperature, the combined Flory−Huggins parameter χN is about 30,[50,51] which corresponds to the intermediate segregation regime.[52]

Scanning Force Microscopy (SFM). The microdomain morphology, the terrace heights, and the absolute film thickness were measured with a Dimension 3100 Metrology SFM (Digital Instruments, Veeco Metrology Group) operated in TappingMode by using silicon tips with a spring constant of 40 N/m and a resonance frequency in the range between 200 and 300 kHz. The Metrology

SFM is based on a hardware-linearized piezoscanner, which compensates for the signal distortions in the *x*, *y*, and *z* directions and allows measurements of distances and heights with a nanometer resolution. The measurements of the phase images were performed at free amplitudes of about 30−50 nm and a relative setpoint of ~0.95. The phase contrast is well resolved at room temperature at a scale of 10−20° due to the different mechanical properties of the PS (glassy) and PB (soft) components. With the TM SFM operated under the above tapping condition, the upper liquid PB layer can be tapped through, and thus the glassy PS structures underneath the PB wetting layer can be imaged.[53]

Special attention was paid to the measurements of the absolute and relative terrace heights. The film thickness was measured with 1−2 nm resolution by processing SFM images of scratches applied to the polymer film with a scalpel. One-layer-thick SB films have an averaged inherent roughness of ~2−3 nm, increasing to ~3−4 nm for the thicker films. There are two important issues to consider: the quality of the raw data and the plane fitting of the raw images. We kept a large scan size (20−30 μm) along the fast scanning axis. The aspect ratio of the images was 1:8 to minimize the distortion of the accumulating signal along the slow scanning axis due to the thermal drift. Background subtraction was done by fitting a plane to the bare substrate. A relative setpoint of ~0.99 was used for the absolute height measurements.

Optical Microscopy. Optical microscopy was used to investigate the characteristic surface topography in annealed SB films (Axiotech microscope from Carl Zeiss AG combined with a digital camera having a resolution of 752 × 582 pixels). When a thin polymer film on a reflective substrate is illuminated with white light, the light is reflected at the substrate and at the film's free surface. The color of the reflected light depends on the local film thickness. As-cast films of each thickness are characterized by an individual uniform color. Upon thermal annealing above the T_g of PS, the microdomains adopt an orientation parallel to the substrate plane and form terraces of well-defined thickness, which are referred to as T_0, $T_{1/2}$, T_1, T_2, etc. The initially smooth surface topography is preserved whenever the film thickness h_o corresponds to an integer number of layered structures (terrace T_n). In all the other cases, the optical images reveal areas of two distinct colors, corresponding to the coexistence of terraces T_n and T_{n+1}, each with a well-defined local film thickness.

Results

The Development of Regions with Equilibrium Thickness. To follow the effect of the polymer−substrate interaction on the structure formation, a series of samples with increments of thickness of ~0.5 a_o (where a_o~ 30 nm is the characteristic cylinder spacing) were annealed under identical conditions on the silicon oxide and carbon-coated substrates. The optical images in Figure 2 show representative regions of the surface topography in selected SB films. The surface patterns for the same film thickness differ depending on the type of the substrate.

As seen in Figure 2a, on silicon oxide, a 30 nm (~a_o) thick film forms a single terrace T_1 of a uniform height except in the areas close to the edges of the substrate. In such regions with increasing thickness, the film splits into coexisting terraces T_1−T_2 (light-brown−dark-brown colors) and T_2−T_3 (dark-brown−blue colors) (inset to Figure 2a). In contrast, the surface topography of a 30-nm-thick SB film on a carbon-coated substrate shows the coexistence of light- and dark-brown areas, which we refer to as terraces $T_{1/2}$ and $T1_{1/2}$ (Figure 2b).

The same tendency in the substrate-dependent surface topography is visible in the optical micrographs of thicker SB films (Figure 2c−d). Figure 2c shows the coexisting terraces T_1 and T_2 in an initially 40-nm-thick SB film on the silicon oxide. For comparison, Figure 2d presents the smooth surface topography with terrace $T1_{1/2}$ in a similar 40-nm-thick SB film annealed on a carbon coating. Islands of terrace $T2_{1/2}$ (dark-brown color) are formed in the regions with an artificial thickness gradient (e.g., around a dust particle).

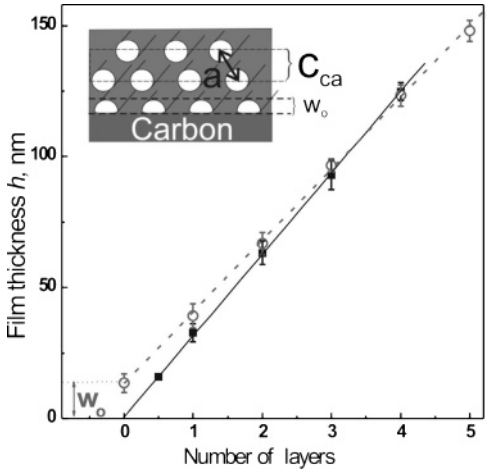

Figure 3. Averaged terrace heights plotted vs the number of layers on carbon-coated (circles) and silicon oxide (squares) substrates. The straight lines are linear fits. The fits' slopes correspond to the mean interlayer distance: $c_{ca} = 27.4 \pm 0.2$ nm and $c_{si} = 31.1 \pm 0.2$ nm on the carbon coating and silicon oxide substrates, respectively. The intercept on the carbon coating indicates a wetting layer of 13.4 ± 0.5 nm, which supports the upper layers. The sketch introduces the analyzed parameters in a film of hexagonally ordered structures.

The difference in terrace formation on the two substrates was observed in up to five layers. The kinetic stability of SB films against dewetting also depends on the type of the substrate. While SB films tend to dewet from the carbon-coated substrate (Figure 2b), no such tendency is observed for the SB films on the silicon oxide surface, which indicates stronger polymer/substrate interaction in the latter case.

We next analyze the equilibrium terrace heights, which are related to the characteristic domain spacing in bulk of the films. In Figure 3, the absolute terrace heights are plotted versus the number of layers. The linear fits differ for the two substrates both in the slope and in the intercept value. The slope of the linear fit corresponds to the vertical periodicity of the layers. On carbon-coated substrates, the averaged interlayer distance c_{ca} is about 27.3 ± 1.4 nm, as expected for hexagonally packed cylinders with a natural spacing a_o of 32.6 ± 0.3 nm, where $c = (\sqrt{3}/2)a$ (Inset to Figure 3). The intercept of the thickness axis indicates a wetting layer of 13.4 ± 0.5 nm supporting all the upper layered structures. Thus the equilibrium terrace heights h_i on the carbon-coated substrate obey the relation $h_i \approx (n + 1/2)c_{ca}$, where n is an integer.

On the silicon oxide, the offset value of the linear fit is close to zero (Figure 3). The equilibrium thickness of a single layer on a silicon oxide is $c_{si} = 31.1 \pm 0.9$ nm, and SB films form a series of stable terraces with $h_i \approx n\ c_{si}$. The value of c_{si} is about 4 nm (~9%) larger than the respective value of c_{ca} on carbon-coated substrates. We shall return to this issue in the discussion section below. Here, we note that such minor differences in the height can be reliably determined only by use of a Metrology SFM.

Phase Behavior on Carbon-Coated Substrates. The SFM images in Figure 4 display the morphological behavior of SB on carbon-coated substrates. The 3D pictures represent both the surface topography and the microdomain structures within each terrace as well as within steps between the terraces. The dominant morphology is a stripe pattern of PS cylinders (white) in a PB matrix (dark). The cylinders are aligned parallel to the plane of the film ($C_{||}$).

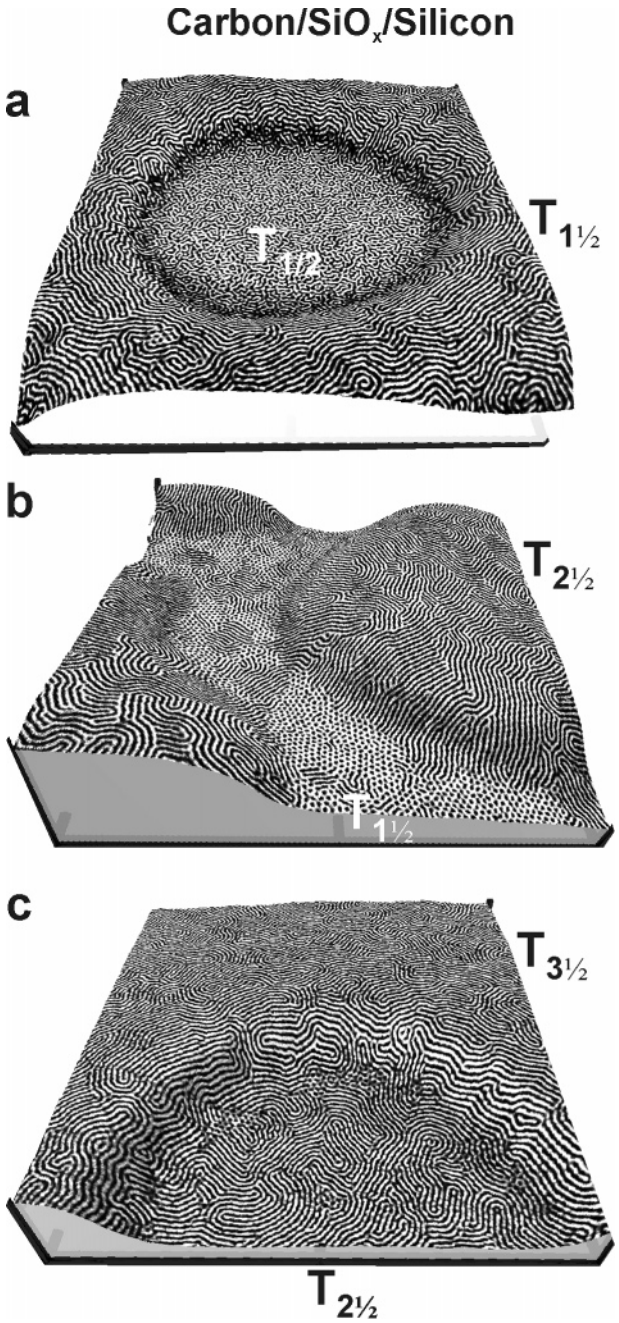

Figure 4. SFM images showing the surface topography and the microdomain structures in SB films on carbon coated substrates. The images were rendered into 3D pictures with Pov-RayTM.[63] The SFM topography images were used as a height field, while the SFM phase signal is represented as a texture. The displayed area is $(3 \times 3 \times 0.06)$ μm^3. The *z*-scale is exaggerated. T_n indicates the terrace number.

Figure 4a shows a hole of terrace $T_{1/2}$ in the majority terrace $T1_{1/2}$, with absolute heights of 14 ± 2 nm and 38 ± 1.5 nm, respectively. Parallel cylinders $C_{||1}$ are exposed to the free surface of terrace $T1_{1/2}$. The microdomain structures in terrace $T_{1/2}$ can be interpreted as half cylinders $C_{||1/2}$. Figure 4b presents terraces $T2_{1/2}$ (66 ± 2 nm) with $C_{||2}$ surface structures separated by a narrow channel of terrace $T1_{1/2}$ (41 ± 2.5 nm) where the two steps overlap. In this area, a pattern of hexagonally ordered dark dots is visible, which we identify as patches of a hexagonally perforated PS lamella (PL).[54] Similar to earlier observations,[24] the PL phase appears preferentially at the bottom of the steps, where the terrace is effectively higher. Figure 4c displays microstructures in the coexisting terraces $T2_{1/2}$ and $T3_{1/2}$ (94 ± 3 nm). Parallel cylinders $C_{||}$ are detected at the surfaces of both terraces. Remarkably, lying cylinders also appear in the regions between the adjacent flat terraces where the thickness deviates from the energetically favored values.

Phase Behavior on Silicon Oxide Substrates. Figure 5 presents the surface structures at favored film thickness on the silicon oxide substrates. The $C_{||1}$ phase is found in terrace T_1 when it is a majority layer (Figure 5a). Nevertheless, in thicker films, the PL_2 phase is repeatedly observed in flat regions, regardless of whether the terrace is an island or a hole. As seen in Figure 5b, the surface structures are represented by a well-ordered PL phase in the neighboring terraces T_2 and T_3 and by the lying cylinders at transition thickness between the terraces. Similarly, Figure 5c displays the PL phase in terrace T_3 and the coexistence of the PL and the $C_{||}$ structures in terrace T_4 and in the step region. The fraction of the $C_{||}$ phase at the transition thickness is considerably larger than that in the flat regions. The step width between terraces T_3 and T_4 is increased as compared to the steps between the lower terraces.

In addition to the $C_{||}$ and the PL structures, Figure 6 presents other phases that appear in silicon oxide-supported films. These are featureless bright areas, characteristic of the lamella (L) phase and morphologically undefined phase-separated pattern, which we refer to as a disordered phase (dis) (terrace T_0 in Figure 6a). Figure 6a shows the characteristic microstructures in an initially 9-nm-thick SB film. The majority of the sample is covered by a disordered layer T_0 with an absolute height of 6 ± 1 nm. Additionally, few islands of terrace T_1 (33 ± 2 nm) with the L_1 phase are formed. In a thicker film (Figure 6b), islands are again characterized by a featureless surface structure, indicative of a lamella phase (L_2). At the same time, the majority T_1 terrace exhibits a coexistence of the $C_{||}$ phase and the randomly perforated L phase. Interestingly, lying cylinders appear at the steps. Figure 6c shows a thicker film where terrace T_2 coexists with terrace T_3. The surface morphology in both terraces is represented by the PL phase. The sequence of small L patches and lying cylinders appears in the region with an intermediate thickness.

The comparison of the surface structures on the silicon oxide (Figures 5−6) and carbon-coated (Figure 4) substrates demonstrates that strong surface interaction significantly changes the phase behavior in the topmost layer. The appearance of the L phase up to the second layer on the strongly interacting substrate is a new experimental result. We emphasize the striking difference compared to the phase behavior of the same block copolymer on the weakly interacting surface.

Discussion

The understanding of the structural developments in substrate-supported films requires explicit analysis of the boundary conditions symmetry. On each of the studied substrates, a lower-surface-energy PB component covers the free surface of SB films with a ~10-nm-thick PB layer.[53] Silicon oxide-supported SB films exhibit symmetric wetting due to the strong interaction of the majority PB block with the substrate (Figure 7). Asymmetric wetting conditions are assumed for the carbon coating, which likely has no preference for SB components.

Upon thermal annealing, the structures align parallel to the film plane, forming up to five distinct layers. Depending on the substrate, the equilibrium terrace heights h_i are $h_i \approx n\, c_{si}$ for symmetric or $h_i \approx (n + {}^1/_2)c_{ca}$ for asymmetric wetting. While surface energetics and related wetting effects have been observed and extensively discussed for thin films of lamella-forming block copolymers,[4] the results presented here are the first confirmation of similar effects in compositionally asym-

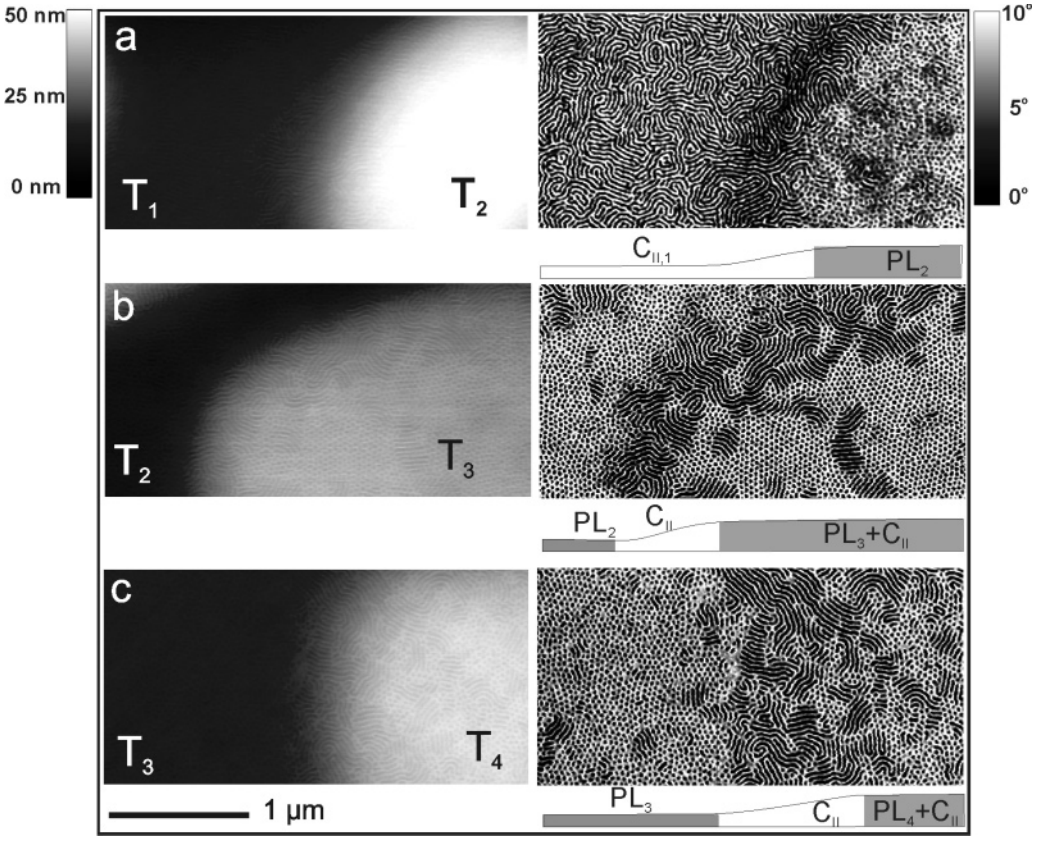

Figure 5. SFM phase and height images ($3 \times 1.5\ \mu m^2$) of the ordered SB films on the silicon oxide substrates. The terrace numbers are indicated in the height images. The sketches below the images illustrate the observed sequence of the morphologies at favored and intermediate thicknesses.

metric block copolymers. To our knowledge, a substrate-induced half-period shift in the layering of cylindrical domains has not been reported before.

Variation of the preferential interaction of the block copolymer components with the substrate provides important insight into the microdomain ordering in thin films. For cylinder-forming block copolymers, this has been studied in detail theoretically,[37,38,40−42,55,56] but seldom experimentally. Before we proceed to the discussion of the phase behavior, we shall briefly touch upon the issue of thermal equilibrium. Equilibration of microdomains by thermal annealing was done on a time scale of about 20 h. According to earlier studies[14] and our own observations, this time period is sufficient for the alignment of the SB microdomains parallel to the substrate and for the development of the equilibrium terrace heights. On longer time scales, the pattern of terraces is still coarsening. This process is driven by the effective line tension between the neighboring terraces. However, on a smaller length scale (~100 nm), the film thickness can be considered constant. Moreover, our in situ studies on the microdomain dynamics in SB films have demonstrated that the characteristic times of microdomain ordering and defect annihilation on a μm scale range from seconds to hours, even at a lower annealing temperature (105 °C).[57] These observations suggest that the microdomain morphologies, which are found within the terraces represent equilibrium phases.

Mapping of the microdomain morphologies to the local film thickness was used to construct the phase diagram of the surface structures as a function of the film thickness and the strength of the surface field at the substrate (Figure 8). Gray areas mark the averaged borders of the equilibrium terrace heights where the favorable morphologies developed (data taken from Figure 3). The white regions indicate the transition thicknesses (steps between the terraces). The black curves are drawn as a guide to the eye in line with the phase boundaries predicted by DDFT simulations.[38,40,41,56]

The generally observed equilibrium microstructures on the carbon coating are cylinders that are aligned parallel to the substrate, as expected from the bulk phase behavior. The $C_{||1/2}$ phase forms in ultrathin films (with h below a_o, Figure 8, image a) and is likely to develop in the bottom layer of thicker films. These structures satisfy the nonpreferential interactions of the SB components with the substrate (Figure 7). Indeed, on a nearly neutral noninteracting substrate (such as carbon coating), the lower surface energy PB component enriches at the solid surface. At the same time, Monte Carlo simulations suggest that an energetically neutral surface exhibits a slight entropic preference to the shorter block (PS in our case) due to the enrichment of chain ends near the hard wall.[55] Stabilization of the $C_{||1/2}$ structures at the substrate has been not observed in experiments. The only indication of transient $C_{||1/2}$ structures was reported in the study of the free surface evolution on a strongly interacting substrate.[22]

The nonbulk PL phase appears only in terrace $T1_{1/2}$ at unfavorable film thickness, either at the bottom of a step (Figure 4b) or in areas with minor thickness variations (Figure 8, image e). Earlier studies[20,24] and the results presented here suggest that the PL phase has a larger interlayer thickness compared to the $C_{||}$ structures. Presumably, the transition from the $C_{||}$ to the PL phase provides a local adjustment of the film structure to the minor thickness variations within one layer.

On the silicon oxide substrates, the $C_{||}$ morphology was observed only at favored thickness in the first layer and in all step regions. Intriguingly, the PL phase was not observed in terrace T_1, although it satisfies the symmetric wetting conditions and is largely represented in higher terraces. The L morphology

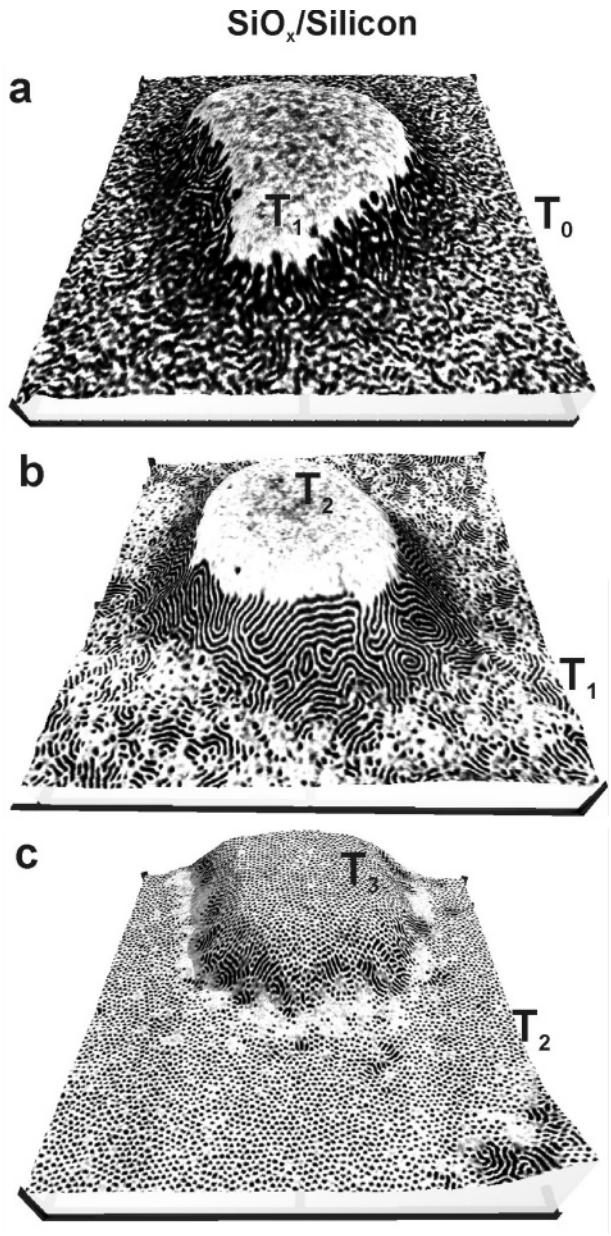

Figure 6. 3D pictures (created as in Figure 4) showing the surface topography and the microdomain structures in SB films on silicon oxide substrates: (a) in coexisting terraces T_0 and T_1 with absolute terrace heights of (6 ± 1 nm) and (33 ± 2 nm), respectively, (b) in terraces T_1 (32 ± 2.5 nm) and T_2 (64 ± 2 nm), and (c) in terraces T_2 (59 ± 2.5 nm) and T_3 (88 ± 3.5 nm). The displayed area is ($3 \times 3 \times 0.06$) μm^3.

Figure 7. Sketches introducing symmetric wetting of the silicon substrate and the free surface by the PB (dark) component (left sketch) and asymmetric wetting conditions on the carbon coating (right sketch).

was detected in islands of terraces T_1 and T_2. This observation, together with the detailed analysis of the sequence of structures in the steps (Figure 4b), suggests that the L phase forms in slightly thicker films due to the higher L domain period than that of the PL phase (Figure 8, image f). In agreement with the simulated phase diagrams,[54,56] with increasing film thickness, the borderlines of the observed PL and L phases shift to the stronger surface fields (Figure 8).

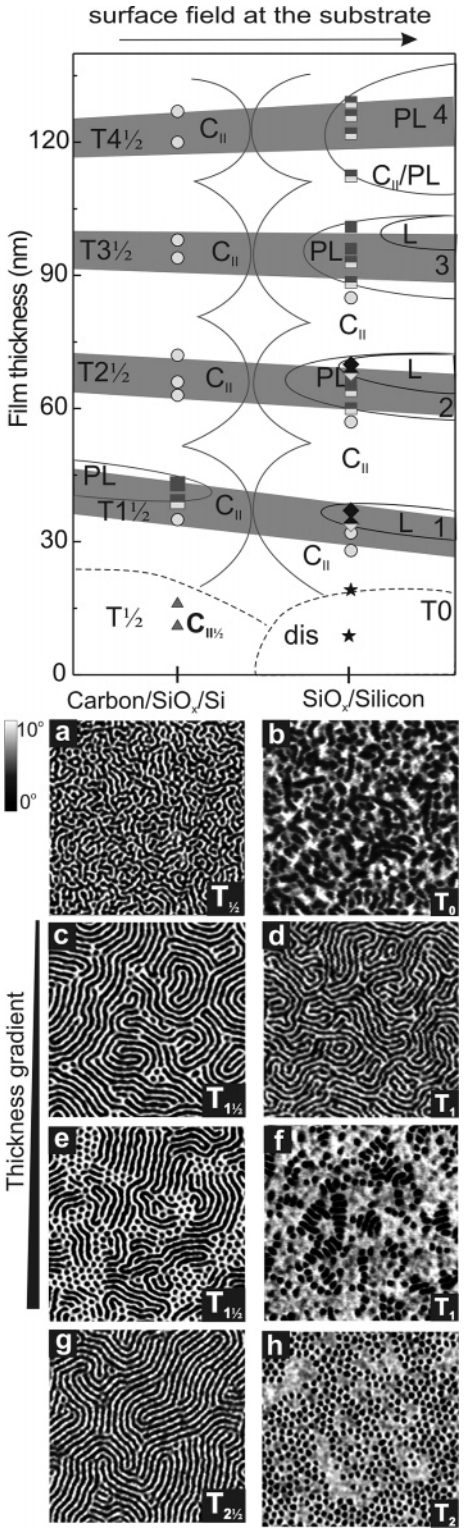

Figure 8. The phase diagram of the surface structures on a weakly interacting surface (carbon coating) and under strong surface field with a preference for the majority component (silicon oxide). Gray areas mark the borders of the preferred film thickness (data taken from Figure 3). The SFM phase images (1×1 μm^2) present examples of the surface structures on carbon-coated (left column) and silicon oxide (right column) substrates at the indicated film thickness. Symbols indicate the following morphologies: circles, the C_{II} phase (images c,d); squares, the PL phase; half-filled squares, coexisting C_{II}/PL structures (image e); diamonds, the L phase; half-filled diamonds, coexisting C_{II}/L patches (image f) or coexisting PL/L microdomains (image h); triangles, $C_{II1/2}$ structures (image a); stars, the disordered phase (image b). Black curves schematically contour the phase boundaries and are drawn as a guide to the eye in line with the DDFT simulations.[38,40,41,56]

The stabilization of the nonbulk structures in the uppermost layer on the silicon oxide, as well as a discrepancy of 10% in the layer thickness on the two substrates, implies that the strong surface field induces the phase transition throughout the SB films. In fact, Matsen predicted[58] that the cylinder-to-PL phase transition is accompanied by an increase of 10% in the microdomain spacing. Recently, the nonbulk PL phase has been observed in up to six layers of structures in bulk-cylinder-forming polystyrene-*block*-poly(methyl methacrylate) copolymer.[25] The authors postulated that the substrate-induced reorganization may be responsible for the formation of the PL structure, which templates from the flat surface.

At transition film thickness on both substrates, lying cylinders have been observed. A thickness-insensitive morphological behavior in steps, where the microstructures have to adjust to the thickness constraint, is a remarkable observation.[62] Both simulated[38,43,55,56] and experimental[24] phase diagrams show broad regions of stability for perpendicularly oriented cylinders independent of the film's thickness on the neutral surfaces and at transition film thickness on strongly interacting substrates. At the same time, the standing cylinders rarely terminate with the $C_{||1/2}$ structures, as only narrow areas of stability are predicted for the latter phase.[38,43,55,56] Additionally, earlier experiments on cylinder-forming block copolymers have shown a variety of morphologies at transition thickness such as standing cylinders,[24,54] spheres,[26,59] PL phase,[20,24,54] cylinders with necks,[60] and more complicated structures.[49,61] Recently, the phase behavior of an SBS triblock copolymer, a morphological analogue of the SB diblock copolymer, was investigated in solvent-swollen films. Depending on the film thickness and the solvent volume fraction, SBS exhibited the PL phase and the cylinders oriented perpendicular to the surface between the neighboring terraces.[24]

The rich morphological behavior and the stabilization of nonbulk morphologies on the silicon oxide substrates is the manifestation of the surface field effects. A strongly interacting substrate affects the enthalpic interactions of the adsorbed monomers[44] and thus enlarges the incompatibility of the block copolymer components. This assumption is supported by the comparison of structures in ultrathin ($h \sim {}^1/_2\, a_o$) SB films. The $C_{||1/2}$ structures on a weakly interacting surface (Figure 8, image a) are characterized by the natural SB microdomain spacing, an extended interface with well-defined interfacial curvature. The disordered pattern on silicon oxide substrates (Figure 8, image b) cannot be attributed to a distinct morphology and suggests stronger segregation on the interacting substrate. Also, the $C_{||}$ microdomains on the silicon oxide (Figure 8, image d) are characterized by less order and higher density of defects as compared to the $C_{||}$ structures on the carbon coating (Figure 8, image c). Presumably, at constrained thicknesses and effectively shifted interaction parameter, the L morphology is stabilized due to the intrinsic instability of the PL structures at the surface-modified segregation regime.

Conclusions

The phase behavior in thin films of a cylinder-forming diblock copolymer melt shows clear dependence on the type of the substrate. On the nearly neutral substrate (carbon-coated silicon) under asymmetric wetting conditions, cylinders are aligned parallel to the surface ($C_{||}$), both at the energetically favored thickness and at the transition thickness. The interlayer distance is consistent with the bulk spacing of the SB cylindrical microdomains. Half cylinders are stabilized at the bottom of the films, reflecting no preference of the SB components to the substrate.

Under the strong surface field and symmetric wetting conditions, the perforated lamella (PL) phase is typically developed in up to four layers. The $C_{||}$ phase was found only in the first layer of structures at the favored film thickness and at all transition regions. Thickness-induced phase transition from the $C_{||}$ to the lamella (L) structures is attributed to the increased incompatibility of the SB components when PB block is strongly attracted to the substrate.

The sequence of structures at transition thickness (in between the steps) suggests a few percent increase of the characteristic microdomain spacing in the order $C_{||}$−PL−L. Comparison of interlayer distances on two types of substrates points to lamella-like structures in the bulk of the films on the strongly interacting surface.

Acknowledgment. This work was supported by the Deutsche Forschungsgemeinschaft (SFB 481; B7). L.T. acknowledges the support of the State of Bavaria (HWP-Program). The support of the VolkswagenStiftung is gratefully acknowledged (R.M.). We thank A. Zvelindovsky and G. J. A. Sevink for fruitful discussions and A. Böker, K. Schmidt, and T. M.Weiss for performing the SAXS measurements.

References and Notes

(1) Hamley, I. W. *The Physics of Block Copolymers*; Oxford University Press: Oxford, 1998.
(2) Krausch, G. *Mater. Sci. Eng., R* **1995**, *14*, 1−94.
(3) Matsen, M. W. *Curr. Opin. Colloid Interface Sci.* **1998**, *3*, 40−47.
(4) Fasolka, M. J.; Mayes, A. M. *Annu. Rev. Mater. Res.* **2001**, *31*, 323−355.
(5) Green, P. F.; Limary, R. *Adv. Colloid Interface Sci.* **2001**, *94*, 53−81.
(6) Thurn-Albrecht, T.; Schotter, J.; Kastle, G. A.; Emley, N.; Shibauchi, T.; Krusin-Elbaum, L.; Guarini, K.; Black, C. T.; Tuominen, M. T.; Russell, T. P. *Science (Washington, D.C.)* **2000**, *290*, 2126−2129.
(7) Li, R. R.; Dapkus, P. D.; Thompson, M. E.; Jeong, W. G.; Harrison, C.; Chaikin, P. M.; Register, R. A.; Adamson, D. H. *Appl. Phys. Lett.* **2000**, *76*, 1689−1691.
(8) Park, M.; Harrison, C.; Chaikin, P. M.; Register, R. A.; Adamson, D. H. *Science (Washington, D.C.)* **1997**, *276*, 1401−1404.
(9) Park, C.; Yoon, J.; Thomas, E. L. *Polymer* **2003**, *44*, 6725−6760.
(10) Segalman, R. A. *Mater. Sci. Eng., R* **2005**, *48*, 191−226.
(11) Mansky, P.; Chaikin, P.; Thomas, E. L. *J. Mater. Sci.* **1995**, *30*, 1987−1992.
(12) Coulon, G.; Russell, T. P.; Deline, V. R.; Green, P. F. *Macromolecules* **1989**, *22*, 2581−2589.
(13) Maaloum, M.; Ausserre, D.; Chatenay, D.; Coulon, G.; Gallot, Y. *Phys. Rev. Lett.* **1992**, *68*, 1575−1578.
(14) Collin, B.; Chatenay, D.; Coulon, G.; Ausserre, D.; Gallot, Y. *Macromolecules* **1992**, *25*, 1621−1622.
(15) Fasolka, M. J.; Banerjee, P.; Mayes, A. M.; Pickett, G.; Balazs, A. C. *Macromolecules* **2000**, *33*, 5702−5712.
(16) Karim, A.; Singh, N.; Sikka, M.; Bates, F. S.; Dozier, W. D.; Felcher, G. P. *J. Chem. Phys.* **1994**, *100*, 1620−1629.
(17) Liu, Y.; Zhao, W.; Zheng, X.; King, A.; Singh, A.; Rafailovich, M. H.; Sokolov, J.; Dai, K. H.; Kramer, E. J.; Schwarz, S. A.; Gebizioglu, O.; Sinha, S. K. *Macromolecules* **1994**, *27*, 4000−4010.
(18) Singh, N.; Kudrle, A.; Sikka, M.; Bates, F. S. *J. Phys. II* **1995**, *5*, 377−396.
(19) van Dijk, M. A.; van den Berg, R. *Macromolecules* **1995**, *28*, 6773−6778.
(20) Radzilowski, L. H.; Carvalho, B. L.; Thomas, E. L. *J. Polym. Sci., Part B: Polym. Phys.* **1996**, *34*, 3081−3093.
(21) Lammertink, R. G. H.; Hempenius, M. A.; Vancso, G. J.; Shin, K.; Rafailovich, M. H.; Sokolov, J. *Macromolecules* **2001**, *34*, 942−950.
(22) Kim, H.-C.; Russell, T. P. *J. Polym. Sci., Part B: Polym. Phys.* **2001**, *39*, 663−668.
(23) Krausch, G.; Magerle, R. *Adv. Mater.* **2002**, *14*, 1579−1583.
(24) Knoll, A.; Magerle, R.; Krausch, G. *J. Chem. Phys.* **2004**, *120*, 1105−1116.
(25) Park, I.; Park, S.; Park, H.-W.; Chang, T.; Yang, H.; Ryu, C. Y. *Macromolecules* **2006**, *39*, 315−318.
(26) Yokoyama, H.; Mates, T. E.; Kramer, E. J. *Macromolecules* **2000**, *33*, 1888−1898.
(27) Segalman, R. A.; Schaefer, K. E.; Fredrickson, G. H.; Kramer, E. J.; Magonov, S. *Macromolecules* **2003**, *36*, 4498−4506.

(28) Edwards, E. W.; Montague, M. F.; Solak, H. H.; Hawker, C. J.; Nealey, P. F. *Adv. Mater.* **2004**, *16*, 1315−1319.
(29) Peters, R. D.; Yang, X. M.; Nealey, P. F. *Macromolecules* **2002**, *35*, 1822−1834.
(30) Walton, D. G.; Kellogg, G. J.; Mayes, A. M.; Lambooy, P.; Russell, T. P. *Macromolecules* **1994**, *27*, 6225−6228.
(31) Carvalho, B. L.; Thomas, E. L. *Phys. Rev. Lett.* **1994**, *73*, 3321−3324.
(32) Mansky, P.; Russell, T. P.; Hawker, C. J.; Pitsikalis, M.; Mays, J. *Macromolecules* **1997**, *30*, 6810−6813.
(33) Huang, E.; Russell, T. P.; Harrison, C.; Chaikin, P. M.; Register, R. A.; Hawker, C. J.; Mays, J. *Macromolecules* **1998**, *31*, 7641−7650.
(34) Turner, M. S. *Phys. Rev. Lett.* **1992**, *69*, 1788.
(35) Williams, D. R. M. *Phys. Rev. Lett.* **1995**, *75*, 453−456.
(36) Akabori, K.-i.; Tanaka, K.; Nagamura, T.; Takahara, A.; Kajiyama, T. *Macromolecules* **2005**, *38*, 9735−9741.
(37) Turner, M. S.; Rubinstein, M.; Marques, C. M. *Macromolecules* **1994**, *27*, 4986−4992.
(38) Lyakhova, K. S.; Sevink, G. J. A.; Zvelindovsky, A. V.; Horvat, A.; Magerle, R. *J. Chem. Phys.* **2004**, *120*, 1127−1137.
(39) Podariu, I.; Chakrabarti, A. *J. Chem. Phys.* **2003**, *118*, 11249−11257.
(40) Huinink, H. P.; Brokken-Zijp, J. C. M.; van Dijk, M. A.; Sevink, G. J. A. *J. Chem. Phys.* **2000**, *112*, 2452−2462.
(41) Huinink, H. P.; van Dijk, M. A.; Brokken-Zijp, J. C. M.; Sevink, G. J. A. *Macromolecules* **2001**, *34*, 5325−5330.
(42) Suh, K. Y.; Kim, Y. S.; Lee, H. H. *J. Chem. Phys.* **1998**, *108*, 1253−1256.
(43) Szamel, G.; Muller, M. *J. Chem. Phys.* **2003**, *118*, 905−913.
(44) Fredrickson, G. H. *Macromolecules* **1987**, *20*, 2535−2542.
(45) Harrison, C.; Chaikin, P. M.; Huse, D. A.; Register, R. A.; Adamson, D. H.; Daniel, A.; Huang, E.; Mansky, P.; Russell, T. P.; Hawker, C. J.; Egolf, D. A.; Melnikov, I. V.; Bodenschatz, E. *Macromolecules* **2000**, *33*, 857−865.
(46) Knoll, A.; Horvat, A.; Lyakhova, K. S.; Krausch, G.; Sevink, G. J. A.; Zvelindovsky, A. V.; Magerle, R. *Nat. Mater.* **2004**, *3*, 886−891.
(47) Ludwigs, S.; Schmidt, K.; Stafford, C. M.; Amis, E. J.; Fasolka, M. J.; Karim, A.; Magerle, R.; Krausch, G. *Macromolecules* **2005**, *38*, 1850−1858.
(48) Brandrup, J., Immergut, E. H., Grulke, E. A., Eds. *Polymer Handbook*, 4th ed.; J. Wiley & Sons: New York, 1999.
(49) Harrison, C.; Park, M.; Chaikin, P. M.; Register, R. A.; Adamson, D. H.; Yao, N. *Polymer* **1998**, *39*, 2733−2744.
(50) Owens, J. N.; Gancarz, I. S.; Koberstein, J. T.; Russell, T. P. *Macromolecules* **1989**, *22*, 3380−3387.
(51) Sakurai, S.; Mori, K.; Okawara, A.; Kimishima, K.; Hashimoto, T. *Macromolecules* **1992**, *25*, 2679−2691.
(52) Bates, F. S.; Fredrickson, G. H. *Annu. Rev. Phys. Chem.* **1990**, *41*, 525−557.
(53) Knoll, A.; Magerle, R.; Krausch, G. *Macromolecules* **2001**, *34*, 4159−4165.
(54) Knoll, A.; Horvat, A.; Lyakhova, K. S.; Krausch, G.; Sevink, G. J. A.; Zvelindovsky, A. V.; Magerle, R. *Phys. Rev. Lett.* **2002**, *89*, 035501−035501/035504.
(55) Wang, Q.; Nealey, P. F.; de Pablo, J. J. *Macromolecules* **2001**, *34*, 3458−3470.
(56) Horvat, A.; Lyakhova, K. S.; Sevink, G. J. A.; Zvelindovsky, A. V.; Magerle, R. *J. Chem. Phys.* **2004**, *120*, 1117−1126.
(57) Tsarkova, L.; Knoll, A.; Magerle, R. submitted.
(58) Matsen, M. W.; Bates, F. S. *J. Chem. Phys.* **1997**, *106*, 2436−2448.
(59) Harrison, C.; Park, M.; Chaikin, P.; Register, R. A.; Adamson, D. H.; Yao, N. *Macromolecules* **1998**, *31*, 2185−2189.
(60) Konrad, M.; Knoll, A.; Krausch, G.; Magerle, R. *Macromolecules* **2000**, *33*, 5518−5523.
(61) Zhang, Q.; Tsui, O. K. C.; Du, B.; Zhang, F.; Tang, T.; He, T. *Macromolecules* **2000**, *33*, 9561−9567.
(62) Very similar phase behavior in transition regions was observed in SB films equilibrated in the solvent vapor. In that case, the hybrid structures such as cylinders with necks are oriented towards the substrate, exposing defect-free cylinders to the free surface. Tsarkova et al. (in preparation).
(63) POV−Team. http://www.povray.org.

MA060224N